




Article

Novel Broadband Slot-Spiral Antenna for Terahertz Applications

Zhen Huang ^{1,2} , Zhaofeng Li ^{1,3,4} , Hui Dong ^{1,5}, Fuhua Yang ^{3,4,6}, Wei Yan ¹ and Xiaodong Wang ^{1,3,4,7,8,*} 

- ¹ Engineering Research Center for Semiconductor Integrated Technology, Institute of Semiconductors, Chinese Academy of Sciences, Beijing 100083, China; zhenhuang@semi.ac.cn (Z.H.); lizhaofeng@semi.ac.cn (Z.L.); dh0511@semi.ac.cn (H.D.); yanwei@semi.ac.cn (W.Y.)
- ² College of Materials Science and Opto-Electronics Technology, University of Chinese Academy of Sciences, Beijing 100049, China
- ³ Center of Materials Science and Optoelectronics Engineering, University of Chinese Academy of Sciences, Beijing 100049, China; fhyang@semi.ac.cn
- ⁴ School of Microelectronics, University of Chinese Academy of Sciences, Beijing 100049, China
- ⁵ The Department of Electronic Science and Technology, University of Science and Technology of China, Hefei 230026, China
- ⁶ State Key Laboratory for Superlattices and Microstructures, Institute of Semiconductors, Chinese Academy of Sciences, Beijing 100083, China
- ⁷ Beijing Academy of Quantum Information Science, Beijing 100193, China
- ⁸ Beijing Engineering Research Center of Semiconductor Micro-Nano Integrated Technology, Beijing 100083, China
- * Correspondence: xdwang@semi.ac.cn

Abstract: We report a novel broadband slot-spiral antenna that can be integrated with high-electron-mobility transistor (HEMT) terahertz (THz) detectors. The effect of various antenna parameters on the transmission efficiency of the slot-spiral structure at 150–450 GHz is investigated systematically. The performances of the slot-spiral antenna and the spiral antenna both integrated with HEMTs are compared. The results show that the slot-spiral structure has a better transmission and miniaturization capability than the spiral structure. A formula for the responsivity is derived based on the transmission line principle and antenna theory, and results show that the detector responsivity is correlated with the antenna absorptivity. Additionally, guidelines for HEMT THz detector design are proposed. The results of this study indicate the excellent application prospects of the slot-spiral antenna in THz detection and imaging.

Keywords: terahertz detector; broadband antenna; slot-spiral; high-electron-mobility transistor; antenna design; responsivity



Citation: Huang, Z.; Li, Z.; Dong, H.; Yang, F.; Yan, W.; Wang, X. Novel Broadband Slot-Spiral Antenna for Terahertz Applications. *Photonics* **2021**, *8*, 123. <https://doi.org/10.3390/photronics8040123>

Received: 23 February 2021

Accepted: 12 April 2021

Published: 14 April 2021

Publisher's Note: MDPI stays neutral with regard to jurisdictional claims in published maps and institutional affiliations.



Copyright: © 2021 by the authors. Licensee MDPI, Basel, Switzerland. This article is an open access article distributed under the terms and conditions of the Creative Commons Attribution (CC BY) license (<https://creativecommons.org/licenses/by/4.0/>).

1. Introduction

Terahertz (THz) radiation (which is broadly defined within the 0.1–10 THz frequency range) has been increasingly studied for radiosopic testing [1,2], nondestructive biopsies [3,4], high-frequency communication [5,6], ultrahigh temporal resolution observation [7,8], etc. Investigating emission and detection over the THz range is more challenging than studying optics and electronics. It is difficult to obtain a high sensitivity and rapid response at room temperature for THz detectors, for which the fundamental operation is based on the conversion of optical signals into electrical signals. These problems have been efficiently solved by using field-effect transistor THz detectors, which have become good candidates for applications. The so-called self-mixing theory was first presented by Dyakonov and Shur in early 1990s [9,10] and has been used to describe the mechanism of THz detection. The asymmetrical coupling of the THz field to a transistor results in AC voltage (V_a) at the terminals of the gate and source [11]. A two-dimensional electron gas (2DEG) exhibits hydrodynamic behavior as a whole and forms a plasma wave. The gate voltage (V_{gs}) approaches the pinch off value. The nonlinear property of the plasma wave in the channel

rectifies the AC signal such that a DC signal (ΔU) can be detected at the output port. The above detection process is illustrated schematically in the right panel of Figure 1.

Although many studies have been performed based on this principle, high responsivity remains difficult to achieve because of the low coupling efficiency between the detector and the incident THz wave. There are three ways to improve the responsivity of field-effect transistor THz detectors. The first one is to replace the traditional gate structure with the grating-gate structure [12], and the second method is to adopt silicon lens or medium-size dielectric cube [13], and the last one is to integrated antenna structure or array structure [14]. Especially for antenna structures, an appropriately designed planar antenna can remarkably enhance the coupling efficiency to improve detector responsivity. A variety of antennas have been employed to date, the most commonly used of which are the dipole [15], bow-tie [16–21], patch [22–25], loop [26], and etc. [27–30]. The above antennas are used in linear polarized THz detection. However, for circularly polarized or non-polarized broadband detection, spiral antennas are usually adopted [31–33]. Here, we propose the slot-spiral antenna integrated HEMT THz detector. This structure has better performance than the spiral structure in circularly polarized or non-polarized broadband detection. The simulation results show that the slot spiral structure not only has the broadband characteristic of a spiral structure but also can improve the responsivity of THz detectors by nearly two orders of magnitude greater than the spiral structure.

In this paper, the numerical simulation results of slot-spiral antenna integrated with HEMT are presented. This paper is organized as follows. Section 2 shows the detection model and specific parameters. Section 3 presents the theoretical analysis of THz responsivity. Section 4 shows the simulation results and discussion about the slot-spiral structure. Section 5 makes detailed discussions about the comparison between slot-spiral antenna with spiral antenna. Section 6 concludes this paper.

2. Detection Model

Considering detection and imaging applications, the simulations were mainly carried out at an optimized transmission efficiency with a 150–450 GHz wave radiated by a Backward-Wave Oscillator (BWO), which has an extremely high radiation power in this region. Figure 1 shows the simulation model, which consists of a cylindrical substrate for which the radius is 400 μm and height is 15.24 μm ; a slot-spiral antenna; and a coupling field-effect transistor (shown as a partially enlarged image on the right side). The metal part of the slot-spiral antenna is composed of Ni/Au (20/200 nm), and Ni is the adhesion layer. A HEMT is in the center of the structure shown in Figure 2. Sapphire is the substrate material; it possesses the advantage of excellent electron transport property and could reduce THz absorption loss. Above the sapphire is GaN/AlGaN (1.8 μm /22 nm). The source and drain ohmic contacts are formed by Ti/Al/Ni/Au (20 /120 /55 /45 nm), and the gate is made of Ni/Au (20/200 nm). It is worth mentioning that the transistor and slot-spiral antenna are not wire-connected; this kind of antenna is called floating antennas, which have also been used in THz detection [16]. We adopted the floating antenna structure here to avoid short circuits between the source and drain (or gate).

The near-field electric field distribution and far-field parameters of the structures were accurately obtained by using the commercial program COMSOL. The antenna in the simulation was created using the formulas given below:

$$\begin{cases} x = w\cos(s) \\ y = w\sin(s) \\ s \in (0, n\pi) \end{cases}, \quad \begin{cases} x = g + w\cos(s) \\ y = g + w\sin(s) \\ s \in (0, n\pi) \end{cases} \quad (1)$$

The two curves presented above form a spiral arm, which revolves around the center to create a second spiral arm, where w controls the increase in the distance of one rotation, n is the slot-spiral lap, and g is the slot-spiral width. These three structure parameters

are the main factors that control the properties of the slot-spiral antenna integrated with HEMTs and will be discussed in detail in the following sections.

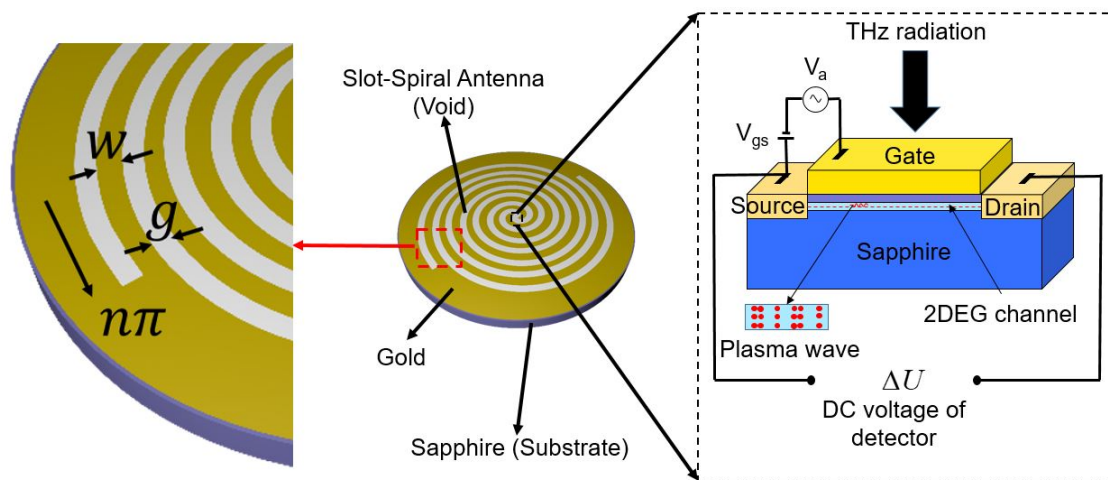


Figure 1. Slot-spiral antenna-coupled field-effect transistor.

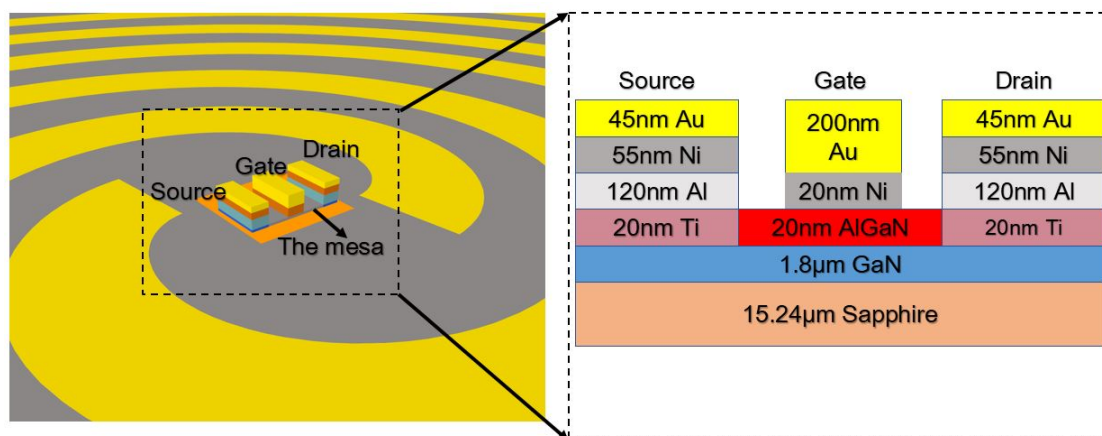


Figure 2. Simulation model of slot-spiral antenna integrated with FET (left) and specific parameters of transistor (right).

3. Terahertz Responsivity

In this section, a formula for the responsivity is derived based on the transmission line principle and antenna theory. This formula considers in detail the influence of various antenna parameters and gives a reasonable explanation of how the antenna affects the responsivity, which is instructive and meaningful to the design of the antenna in THz detectors. Our derivation is based in part on the pioneering work of other researchers.

A leading study by Knap [34,35] performed further crucial analyses on resonant and nonresonant detection, showing the following:

$$\Delta U = \frac{eV_a^2}{4\eta K_B T} \tag{2}$$

This formula is only effective when $V_{GS} < V_{th}$. All parameters related to transistors are taken into account in η . V_a is the AC voltage induced by THz radiation, and it is correlated with radiation frequency, where e is the electron charge, η is the ideality factor (assumed to be 1 in the simulation), K_B is the Boltzmann constant, and T is temperature (300 K at room temperature).

According to antenna theory, the total power that the transistor absorbs from the electromagnetic wave ($P_{Transistor}$) can be calculated as follows [21]:

$$P_{Transistor} = P_{in} \frac{\lambda^2}{4\pi} G_{0abs} \quad (3)$$

In the equations above, P_{in} is the incident power density, λ is the wavelength of electromagnetic wave, and G_{0abs} is the maximum absolute gain. Note that the magnitude of G_{0abs} is equal to the antenna directivity multiplied by the overall efficiency, which contains the conduction, and dielectric and reflection efficiencies [21].

Furthermore, based on the transmission line principle, the power delivered to the transistor can be expressed as given below [21]:

$$P_{Transistor} = \frac{1}{2} V_a^2 \frac{Re\{Z_T\}}{|Z_T|^2} \quad (4)$$

Z_T is the impedance of the transistor. Usually, it is complex to calculate Z_T accurately [36]. We could set Z_T to be 50Ω [21]. Equations (3) and (4) are combined and substituted into Equations (2), and we can obtain a formula for the responsivity (R_V):

$$R_V = \frac{\Delta U}{P_{in} S_{det}} = \frac{e}{8\pi K_B T} \frac{\lambda^2}{S_{det}} \frac{|Z_T|^2}{Re\{Z_T\}} G_{0abs} \quad U_{GS} < U_{th} \quad (5)$$

In the equation above, S_{det} is the area of the THz detector instead of the antenna area. Both detector area and antenna area have been used in the literature; here, we chose the detector area as the effective area.

Different from the computing method we used before, we replaced the radiation intensity with a more referential value maximum absolute gain G_{0abs} . This value is meaningful for the simulation and design of the THz detectors integrated with receiving antenna. By converting the calculated parameter from radiation intensity to G_{0abs} , more accurate calculation results can be obtained.

4. Simulation Results

The results of numerical simulation of slot-spiral antenna integrated with HEMT with different parameters are presented and analyzed in this section. The air domain around the structure is modeled as a cuboid. For the radiation mode of simulation, perfectly matched layer (PML) boundary conditions are applied in all directions [21]. For the receiving mode of simulation in this paper, periodic boundary conditions are applied in the transverse and PML boundary conditions are applied in the vertical directions. The THz plane wave irradiates the model vertically as illustrated in Figure 1. Floating slot-spiral antenna integrated with HEMT is displayed in Figure 2. The absorptivity ($1 - |S_{11}|^2 - |S_{21}|^2$) results from sweeping the three parameters (n , g , and w in Figure 1) are obtained. The analysis results of the three parameters (n , g , and w , respectively) are presented in the following subsections.

4.1. Effect of Slot-Spiral Laps

The slot-spiral laps are varied from 1 to 7, and the other parameters are maintained at $g = w = 15 \mu\text{m}$. The lumped port absorptivity curves versus the frequency are shown in Figure 3. It can be seen that the slot-spiral structure barely transmitted any energy when $n = 1$ and even $n = 2$, where only a fraction of this energy can be transmitted at 350–450 GHz. It is almost impossible for the slot to form a complete frontal helix for these two limiting cases. We can assume that this structure is not a slot-spiral antenna and does not have the same properties as the structure at the other n values. The absorptivity increases with n at the low-frequency stage (150–175 GHz) and remains flat at nearly 90 percent at $n = 7$, with little correlation with the frequency; as an excessively large n dramatically increases the antenna area, an appropriate value of n can improve the bandwidth of the THz detector. Thus, $n = 7$ is suitable for high power detection for the basic frequency power of our THz source.

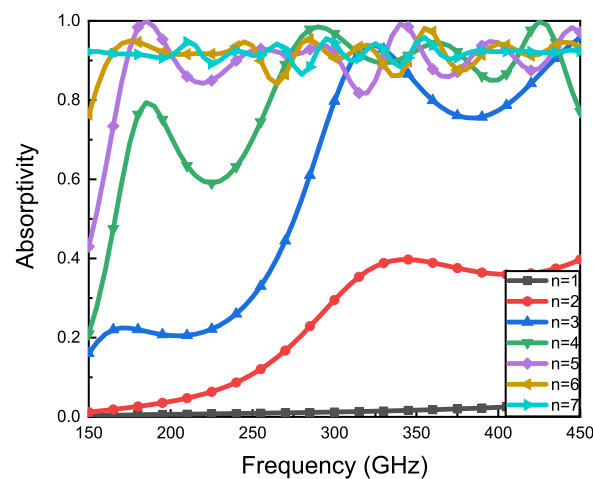


Figure 3. Absorptivity versus frequency with different n (1–7).

In addition to the relationship between the bandwidth and n , we also found a repeatable relationship between absorptivity peak and n (when n is a decimal and between every two integers), which is important for narrow band detection but not significant for broadband detection; we will not present further details here, as the same conclusions have previously been reported [37].

4.2. Effect of Slot-Spiral Width

A universal law for variable slot-spiral widths is reported in this section. To exclude the influence of other parameters, we set $n = 7$ and $w = 15 \mu\text{m}$. A slot-spiral width in the 10–20 μm range was first investigated and then extended to 1–10 μm and 20–40 μm to analyze the limit condition. Figure 4C,D shows a negative correlation between the absorptivity and the slot-spiral width, where different widths have no effect on the peak position of the resonant frequency; that is, the slot-spiral width does not affect the resonance of the antenna but does affect the ability of the antenna to transmit and receive electromagnetic waves. With an increase in g , the resonant peaks become weaker and the curves tend to be flat.

Nevertheless, decreasing the gap is not necessarily better. Figure 4B shows the absorptivity versus the frequency for g in the 5–10 μm range. Reducing the slot gap further does not change the resonant frequency position, whereas the absorptivity of the structure continues to increase; however, some unique features are observed for the absorptivity at $g = 5 \mu\text{m}$. First, the absorptivity does not exhibit exactly the same trend in the frequency as the other curves, and second, the resonance position changes slightly. Figure 4A shows the absorptivity for even narrower slot gaps of 1–5 μm , where the higher g value corresponds to a higher antenna absorptivity, which is opposite to the conclusion above. The curve for $g = 5 \mu\text{m}$ exhibits a different trend from that of the other four curves, which is called the turning point. In this case, the arm width of the slot-spiral antenna is considerably smaller than the other parameters, effectively decreasing the dimension of the antenna and resulting in different characteristics. Considering the requirements of broadband antenna, the slot width is an important parameter that affects the THz detector responsivity and the ideal value of the slot-spiral width is the turning point, which is 5 μm for this THz detector.

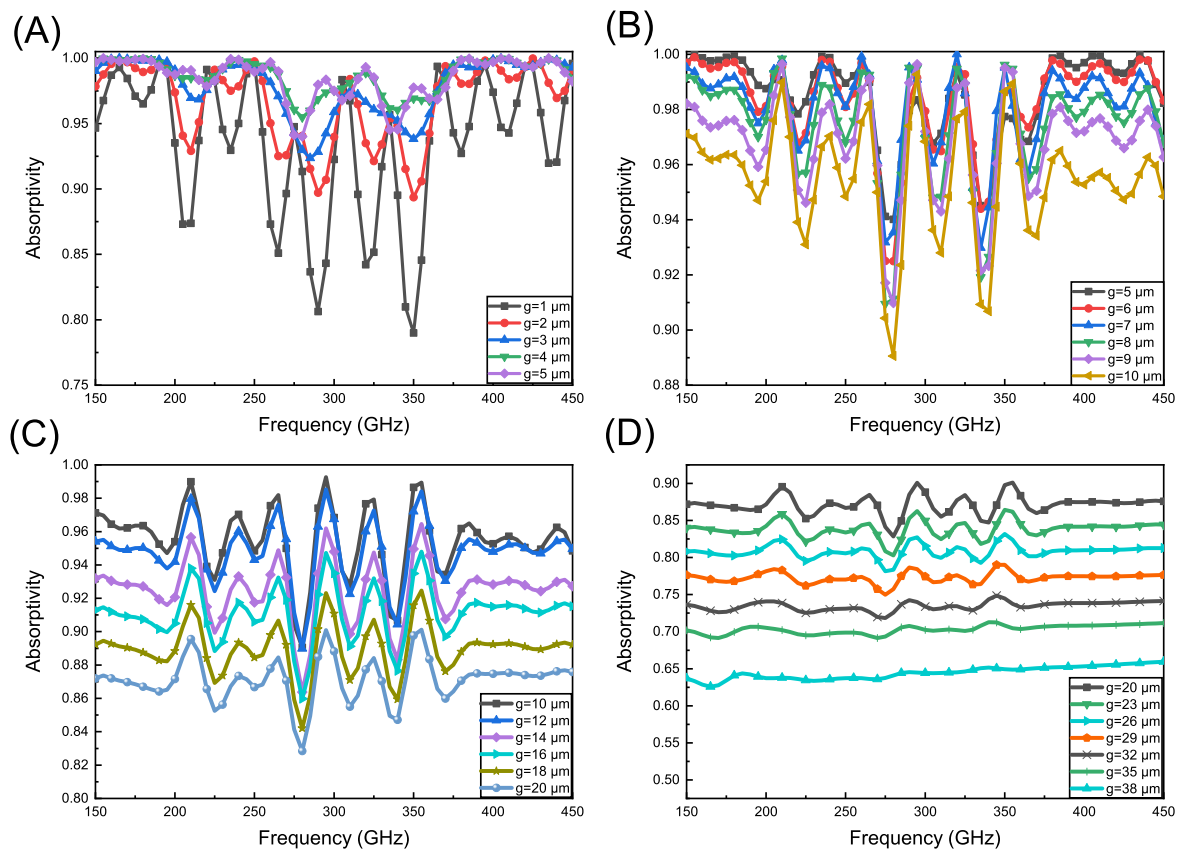


Figure 4. Absorptivity versus frequency with different g : (A) $g = 1\text{--}5\ \mu\text{m}$, (B) $g = 5\text{--}10\ \mu\text{m}$, (C) $g = 10\text{--}20\ \mu\text{m}$, and (D) $g = 20\text{--}38\ \mu\text{m}$.

4.3. Effect of Increasing the Distance of One Rotation

The effect of increasing the distance of one rotation on the properties of the antenna and THz detector is discussed in this section. The curve equation given by Equation (1) shows that w controls the increase in the distance of one rotation. Figure 1A shows the absorptivity versus frequency for different widths (5–12 μm). A peak absorptivity of approximately 1 occurs for every single curve, but the region where the absorptivity distribution above 0.9 is very narrow. The resonant frequency gradually decreases because increasing w results in a larger spiral arm length. This result is more applicable to narrow-band high-responsivity detection than broadband detection. We did not decrease w below 5 because that would have resulted in a nearly invisible spiral gap, reducing the entire model to a disk.

Another important result that can be observed from Figure 5A is that the amplitude of the absorptivity oscillation decreases as w increases. Thus, we extended w in the simulation to 13–20 μm , and the result shown in Figure 5B corroborates our conjecture. Over the 150–450 GHz region, the absorptivity curve exhibits a slowly increasing trend and approaches 1 for gradually increasing w . However, a higher value of w is not very effective at increasing absorptivity but will increase the area of the detector, which is not conducive to the integration of devices; the ideal value could be 15 μm . Overall, increasing the distance of one rotation affects both the resonant frequency of the narrowband antenna and the transmission efficiency of the broadband antenna.

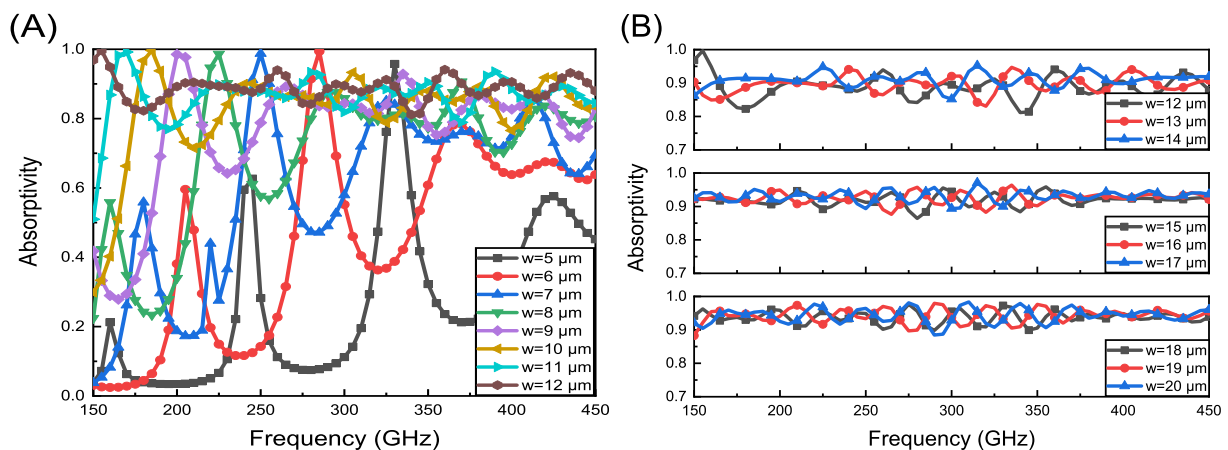


Figure 5. Absorptivity versus frequency with different w: (A) w = 5–12 μm and (B) w = 12–20 μm .

5. Discussions

A comparative analysis of the performances of the spiral structure and the slot-spiral structure is conducted under the same external conditions. One exception is that the void area of the spiral antenna is completely filled with metal, and the original metal area of the spiral antenna is completely removed to form a pattern that is complementary to our structure, as is shown in Figure 6. The only difference between them is whether the outside tails of two arms are connected. Slot-spiral antenna and spiral antenna are both floating, which means that neither are connected to the transistors.



Figure 6. Slot-spiral structure (left) and spiral structure (right) both integrated with high-electron-mobility transistor (HEMT) in the center.

Figure 7 clearly presents the absorptivity for the two structures with the same dimensions. The slot spiral has a higher absorptivity than the spiral, with all other factors the same. Although both structures exhibit the same performance trend when varying the antenna parameters, higher n and w (corresponding to a larger area) are required for the spiral antenna to achieve the same receiving and transmitting abilities as the slot-spiral antenna, which is not conducive for miniaturization of the THz detector.

Considering the antenna energy transmission, the slot-spiral antenna can receive a considerably larger area of electromagnetic waves than the spiral antenna: Figure 8 shows that, for the same dimension and frequency, the electric field is distributed in almost all the gaps on the surface of the slot-spiral antenna, whereas the electric field is funneled into the center of the spiral antenna; the maximum electric field occurs at the center of both antennas with nearly equal values, but the electric field of the slot-spiral antenna is clearly stronger than that of the spiral antenna elsewhere, showing that the novel structure can absorb more energy to transmit to a THz detector, thus effectively improving the responsivity.

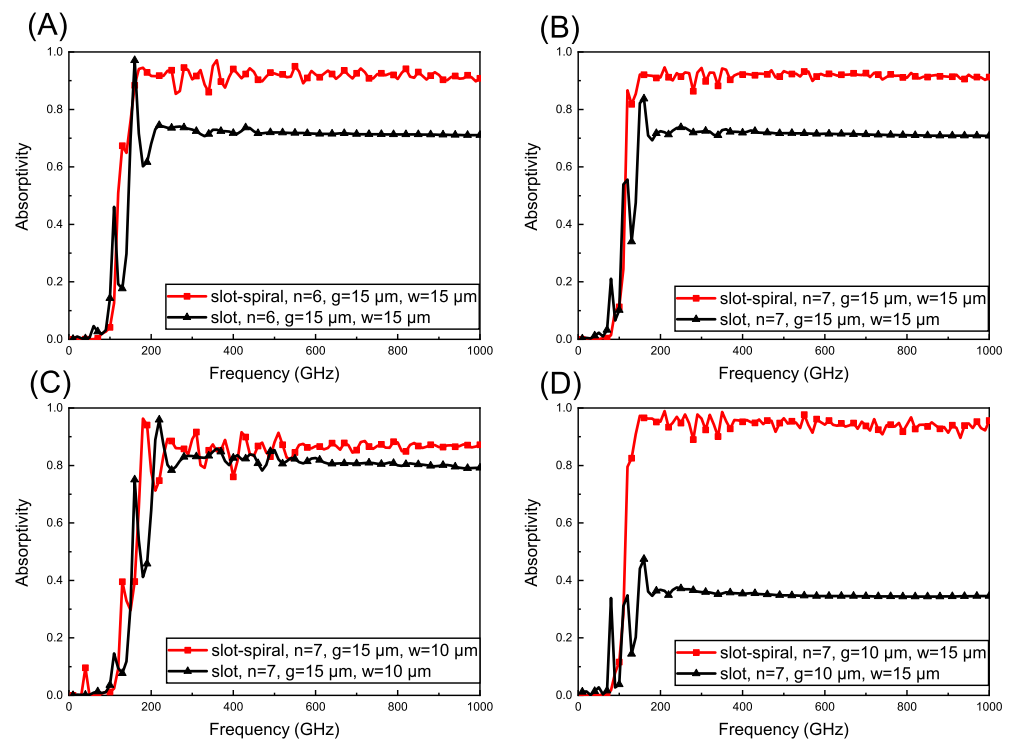


Figure 7. Comparisons of slot-spiral structure with the spiral structure of different structure parameters: (A) $n = 6$, $g = 15 \mu\text{m}$, and $w = 15 \mu\text{m}$; (B) $n = 7$, $g = 15 \mu\text{m}$, and $w = 15 \mu\text{m}$; (C) $n = 7$, $g = 15 \mu\text{m}$, and $w = 10 \mu\text{m}$; and (D) $n = 7$, $g = 10 \mu\text{m}$, and $w = 15 \mu\text{m}$.

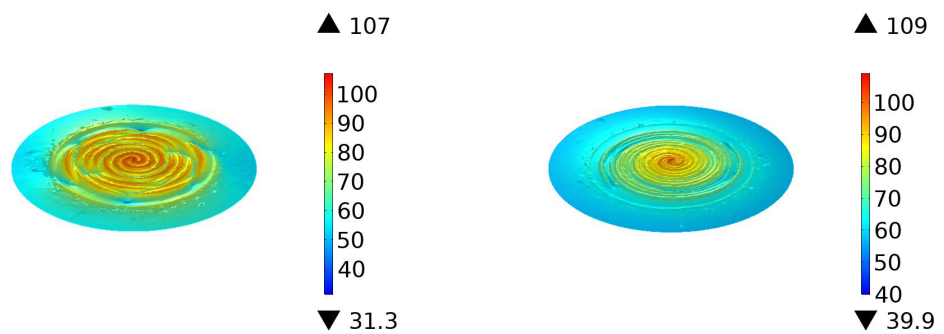


Figure 8. Electric field distribution of the slot-spiral structure (left) and spiral structure (right) at $n = 7$, $w = g = 15 \mu\text{m}$, and 300 GHz.

We also simulate the maximum absorption rate of the slot-spiral antenna at the optimum size, which is $n = 7$, $g = 5 \mu\text{m}$, and $w = 15 \mu\text{m}$, and extended the results to the directivity, absorptivity, G_{0abs} , and R_V , the results of which were compared with the spiral antenna (for which the optimal size is $n = 7$, $g = 15 \mu\text{m}$, and $w = 5 \mu\text{m}$) and shown in Figure 9.

In this case, the novel slot-spiral antenna still shows better performance than the spiral antenna, regardless of parameters (directivity, absorptivity, G_{0abs} , and R_V), and the responsiveness of this novel structure is two orders of magnitude greater than that of spiral structure. The resonant frequency of the slot-spiral antenna and spiral antenna are both near 300 GHz. In the vicinity of this frequency range, the broadband characteristics of both structures are relatively close. However, the slot-spiral antenna is more similar to a slot antenna especially at high frequency, since the metal parts of the slot-spiral antenna are all connected together. When far from the resonant frequency, its broadband characteristics are not as good as that of the spiral antenna. Therefore, in the high frequency range 600–1000 GHz, directivity and gain show a noisy behavior compared with spiral antenna [38–40].

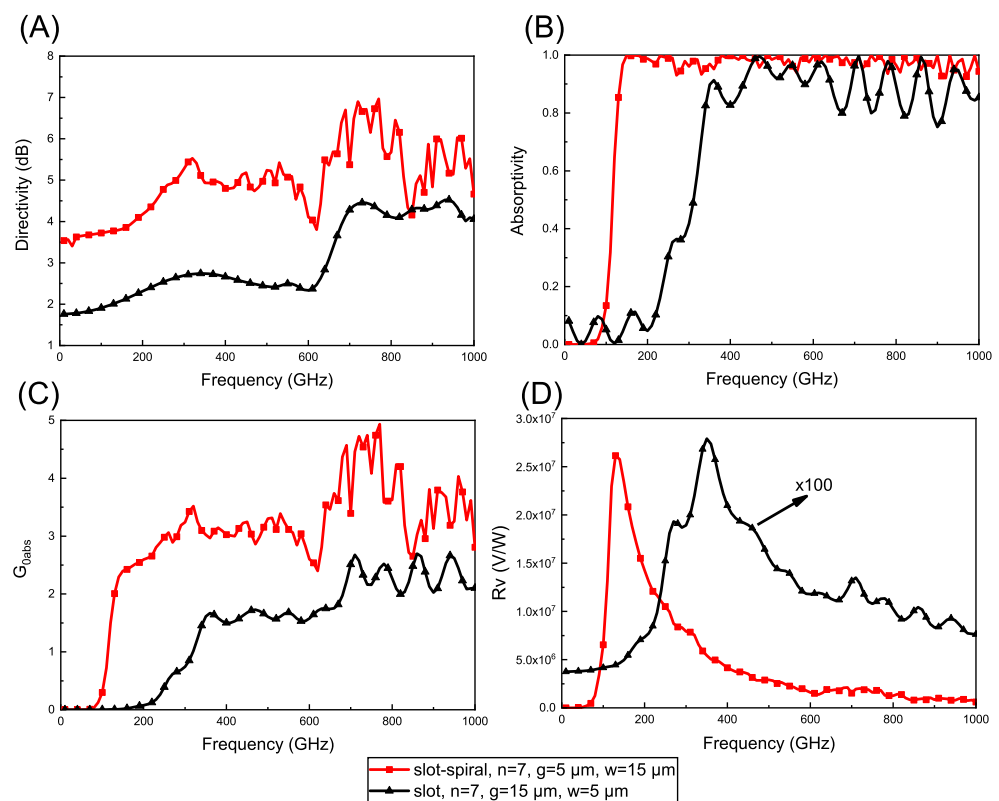


Figure 9. Comparisons of slot-spiral structure and spiral structure: (A) directivity versus frequency, (B) absorptivity versus frequency, (C) G_{0abs} versus frequency, and (D) R_V versus frequency.

Another interesting finding is that the resonant frequency at which the responsivity takes the maximum value is almost the same as the initial frequency at which the absorptivity slope is maximal. The slot-spiral structure does show better performance in THz transmission. Furthermore, it is interesting to mention that, compared with structures designed by others, it is easier for our structure to absorb more than 80 percent of the THz wave over a wide range [37]. Secondly, our new structure could transmit nearly 3 times as much electric field energy as the structure designed by others at 300 GHz [31]. Thirdly, there is no need for our new structure to design multiple layers, which greatly simplifies the fabrication process [32]. Lastly, the connection between HEMT and the slot-spiral antenna is different from other designs, making it easier to form an asymmetric structure [33]. However, what should be emphasized is that the antenna and HEMT are in the same plane, which makes it difficult for the HEMT to connect to the pad. A micro-bridge structure could be designed to connect them from the top of the antenna plane. This kind of structure is a challenge in fabrication, and we will solve the fabrication problems and produce the whole device in the future.

Figure 10 shows the variation in the responsivity and absorptivity versus the antenna parameters (n , g , and w) at different frequencies (200 GHz, 300 GHz, and 400 GHz). The diagram clearly shows the same trend in the absorptivity of the slot-spiral antenna and responsivity of THz detector for a fixed frequency, irrespective of the values of n , g , or w ; however, for the region $w < 5 \mu\text{m}$, different trends in the absorptivity and responsivity are observed for different antenna performances, which has been explained in the preceding analysis of the effects of w on the antenna performance. We re-emphasize that the detector area is used to calculate the responsivity instead of the antenna area, where the detector area is considerably smaller (by nearly 1000 times) than the antenna area, resulting in an apparent large simulated responsivity.

The result that the antenna absorptivity and the THz detector responsivity exhibit the same change trends provides guidance for designing an antenna and a THz detector.

The first three terms in Equation (5) are all fixed values for a given transistor that are independent of the variation in antenna parameters at a specific frequency when the applied bias and temperature are stable. Therefore, attention should be focused on improving the maximum absolute gain, which could be extracted from the simulation directly; at the same time, the resonant frequency of the THz detector also corresponds to that of absorptivity. The absorptivity and G_{0abs} nearly remain the same even when the frequency increases, but the responsivity decreases rapidly; the reason for this result is that, with the increase in frequency, the second team related to the wavelength is reduced, which leads to the decrease in responsivity. It can be seen that this formula could give significant guidelines for designing a THz detector.

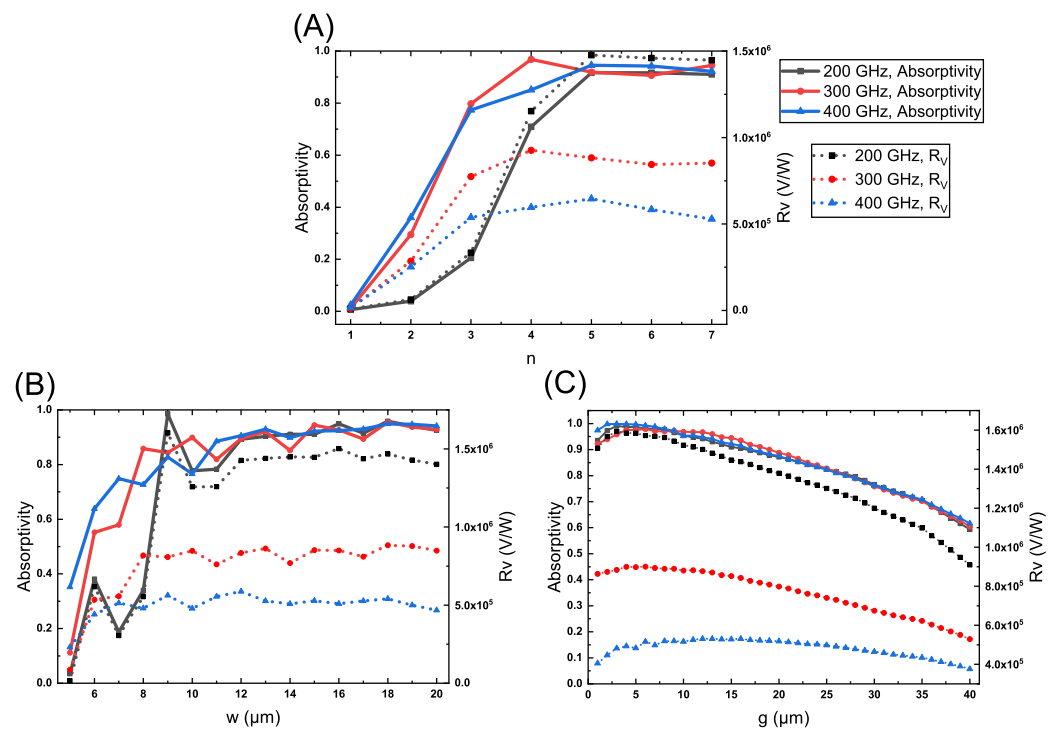


Figure 10. Absorptivity and responsivity versus (A) n, (B) w, and (C) g.

6. Conclusions

We carried out a study on a novel broadband slot-spiral antenna coupled with a THz detector. Based on the BWO output power, the frequency range is fixed in the region between 150-450 GHz. We adopt a novel structure that is complementary to spiral antenna, using the slot as the main part of the antenna. We systematically investigate the effects of various antenna parameters (including the slot-spiral laps, width, and the increase in the distance of one rotation) on the antenna absorptivity and perform a comparative analysis of the performances of the spiral and slot-spiral antennas. The novel structure can be coupled with more electromagnetic power than the spiral antenna with the same dimensions. The traditional structure needs a larger effective area to achieve the same transmission efficiency as the novel structure, showing that the novel structure more easily satisfies increasing miniaturization demands. Ultimately, a formula for the THz responsivity is derived, showing a detector performance with the variation in antenna parameters that is consistent with the absorptivity, presenting an instructive method of antenna design.

This study presents a first step in demonstrating the feasibility of antenna-coupled HEMT THz detectors by employing a novel broadband slot-spiral antenna and notable improvements in transmission and miniaturization. Excellent transmission performance leads to higher responsivity, and the miniaturization characteristic is more conducive to large-scale integration of the device so that imaging can be realized. Only the antenna

parameters have been considered, and other structures, such as pads, wire length [41], and substrates [21,42], have not been taken into account. Note that the gate needs to be placed in the middle of the antenna, forming an asymmetric structure in the actual fabrication. The slot-spiral antenna and HEMT are in the same plane and not directly connected, which makes it difficult for the source, drain, and gate to connect to the pad. A micro-bridge structure could be designed to connect them from the top of the antenna. This kind of structure is a challenge in fabrication, and we will solve the fabrication problems and produce the whole device in the future.

To summarize, aiming at applications in detection and imaging in the frequency range of 150–450 GHz, a novel broadband slot-spiral antenna is designed and investigated; this new structure shows better performance than the spiral structure. There are some problems in process compatibility, and they will be solved in the future when the technological conditions become more mature. Nevertheless, the broad bandwidth and miniaturization performance of this novel structure will be fully developed in the future.

Author Contributions: Conceptualization, Z.H.; methodology, Z.H.; software, Z.H. and Z.L.; formal analysis, Z.H. and Z.L.; investigation, Z.H. and H.D.; data curation, Z.H. and W.Y.; writing—original draft preparation, Z.H.; writing—review and editing, W.Y., X.W., and Z.L.; supervision, F.Y. and X.W.; funding acquisition, Z.L. and W.Y. All authors have read and agreed to the published version of the manuscript.

Funding: This work is partly supported by National Key R&D Program of China under grant 2018YFE0204000 and the National Natural Science Foundation of China (grant No. 61971395).

Institutional Review Board Statement: Not applicable.

Informed Consent Statement: Not applicable.

Data Availability Statement: The data that support the findings of this study are available from the corresponding author upon request.

Conflicts of Interest: The authors declare no conflict of interest.

Abbreviations

The following abbreviations are used in this manuscript:

THz	terahertz
HEMT	high-electron-mobility transistor
2DEG	two-dimensional electron gas
AC	alternating current
DC	direct current

References

1. Ergun, S.; Sonmez, S. Terahertz technology for military applications. *J. Manag. Inf. Sci.* **2015**, *3*, 13–16. [[CrossRef](#)]
2. Xin, Z.; Chao, L. Recent development of THz technology and its application in radar and communication system. *J. Microwaves* **2010**, *26*, 1–6.
3. Siegel, P.H. Terahertz technology in biology and medicine. *IEEE Trans. Microw. Theory Tech.* **2004**, *52*, 2438–2447. [[CrossRef](#)]
4. Pickwell, E.; Wallace, V. Biomedical applications of terahertz technology. *J. Phys. D Appl. Phys.* **2006**, *39*, R301. [[CrossRef](#)]
5. Kürner, T. Towards future THz communications systems. *Terahertz Sci. Technol.* **2012**, *5*, 11–17.
6. Yang, Y.; Mandehgar, M.; Grischkowsky, D.R. Broadband THz pulse transmission through the atmosphere. *IEEE Trans. Terahertz Sci. Technol.* **2011**, *1*, 264–273. [[CrossRef](#)]
7. Benford, D.J.; Amato, M.J.; Mather, J.C.; Moseley, S.H.; Leisawitz, D.T. Mission concept for the single aperture far-infrared (SAFIR) observatory. *Astrophys. Space Sci.* **2004**, *294*, 177–212. [[CrossRef](#)]
8. Siegel, P.H. THz applications for outer and inner space. In Proceedings of the 2006 12th International Symposium on Antenna Technology and Applied Electromagnetics and Canadian Radio Sciences Conference, Montreal, QC, Canada, 17–19 July 2006; pp. 1–4.
9. Dyakonov, M.; Shur, M. Shallow water analogy for a ballistic field effect transistor: New mechanism of plasma wave generation by dc current. *Phys. Rev. Lett.* **1993**, *71*, 2465. [[CrossRef](#)] [[PubMed](#)]

10. Dyakonov, M.; Shur, M. Detection, mixing, and frequency multiplication of terahertz radiation by two-dimensional electronic fluid. *IEEE Trans. Electron Devices* **1996**, *43*, 380–387. [[CrossRef](#)]
11. Gorbenko, I.; Kachorovskii, V.Y.; Shur, M. Terahertz plasmonic detector controlled by phase asymmetry. *Opt. Express* **2019**, *27*, 4004–4013. [[CrossRef](#)]
12. Huang, Y.; Yu, Y.; Qin, H.; Sun, J.; Zhang, Z.; Li, X.; Huang, J.; Cai, Y. Plasmonic terahertz modulator based on a grating-coupled two-dimensional electron system. *Appl. Phys. Lett.* **2016**, *109*, 201110. [[CrossRef](#)]
13. Minin, O.V.; Minin, I.V.; Meziani, Y.M.; Hisatake, S. Improvement of a point-contact detector performance using the terajet effect initiated by photonics. *Opt. Eng.* **2020**, *60*, 082005. [[CrossRef](#)]
14. Öjefors, E.; Lisauskas, A.; Glaab, D.; Roskos, H.G.; Pfeiffer, U.R. Terahertz imaging detectors in CMOS technology. *J. Infrared Millim. Terahertz Waves* **2009**, *30*, 1269–1280. [[CrossRef](#)]
15. Tanigawa, T.; Onishi, T.; Takigawa, S.; Otsuji, T. Enhanced responsivity in a novel AlGaIn/GaN plasmon-resonant terahertz detector using gate-dipole antenna with parasitic elements. In Proceedings of the 68th Device Research Conference, Notre Dame, IN, USA, 21–23 June 2010; pp. 167–168.
16. Sun, J.; Sun, Y.; Wu, D.; Cai, Y.; Qin, H.; Zhang, B. High-responsivity, low-noise, room-temperature, self-mixing terahertz detector realized using floating antennas on a GaN-based field-effect transistor. *Appl. Phys. Lett.* **2012**, *100*, 013506.
17. Yu, M.; Geng, H.; Jiang, S.; Hua, T.; An, D.; Xu, W.; Chen, Z.N.; Li, J.; Wang, H.; Chen, J.; et al. Bowtie loaded meander antenna for a high-temperature superconducting terahertz detector and its characterization by the Josephson effect. *Opt. Express* **2020**, *28*, 14271–14279. [[CrossRef](#)]
18. Zhang, B.W.; Yan, W.; Li, Z.F.; Bai, L.; Cywinski, G.; Yahniuk, I.; Szkudlarek, K.; Skierbiszewski, C.; Przybytek, J.; But, D.B.; et al. An effective method for antenna design in field effect transistor terahertz detectors. *Int. J. Infrared Millim. Waves* **2018**, *37*, 389–392.
19. Ikamas, K.; But, D.B.; Lisauskas, A. Homodyne Spectroscopy with Broadband Terahertz Power Detector Based on 90-nm Silicon CMOS Transistor. *Appl. Sci.* **2021**, *11*, 412. [[CrossRef](#)]
20. Bauer, M.; Rämmer, A.; Chevtchenko, S.A.; Osipov, K.Y.; Čibiraitė, D.; Pralgauskaitė, S.; Ikamas, K.; Lisauskas, A.; Heinrich, W.; Krozer, V.; et al. A high-sensitivity AlGaIn/GaN HEMT terahertz detector with integrated broadband bow-tie antenna. *IEEE Trans. Terahertz Sci. Technol.* **2019**, *9*, 430–444. [[CrossRef](#)]
21. Zhang, B.; Yan, W.; Li, Z.; Bai, L.; Yang, F. Analysis of substrate effect in field effect transistor terahertz detectors. *IEEE J. Sel. Top. Quantum Electron.* **2016**, *23*, 1–7. [[CrossRef](#)]
22. Liu, Z.Y.; Liu, L.Y.; Yang, J.; Wu, N.J. A CMOS fully integrated 860-GHz terahertz sensor. *IEEE Trans. Terahertz Sci. Technol.* **2017**, *7*, 455–465. [[CrossRef](#)]
23. Kopyt, P.; Salski, B.; Zagrajek, P.; Obrębski, D.; Marczewski, J. Modeling of silicon-based substrates of patch antennas operating in the sub-THz range. *IEEE Trans. Terahertz Sci. Technol.* **2017**, *7*, 424–432. [[CrossRef](#)]
24. Xu, L.J.; Tong, F.C.; Bai, X.; Li, Q. Design of miniaturised on-chip slot antenna for THz detector in CMOS. *IET Microwaves Antennas Propag.* **2018**, *12*, 1324–1331. [[CrossRef](#)]
25. Kanazawa, Y.; Yokoyama, S.; Hiramatsu, S.; Sano, E.; Ikegami, T.; Takida, Y.; Ambalathankandy, P.; Minamide, H.; Ikebe, M. Wideband terahertz imaging pixel with a small on-chip antenna in 180 nm CMOS. *Jpn. J. Appl. Phys.* **2019**, *58*, SBBL06. [[CrossRef](#)]
26. Labidi, M.; Choubani, F. Performances enhancement of metamaterial loop antenna for terahertz applications. *Opt. Mater.* **2018**, *82*, 116–122. [[CrossRef](#)]
27. Hou, H.; Liu, Z.; Teng, J.; Palacios, T.; Chua, S.J. A sub-terahertz broadband detector based on a GaN high-electron-mobility transistor with nanoantennas. *Appl. Phys. Express* **2016**, *10*, 014101. [[CrossRef](#)]
28. Mou, J.; Xue, Q.; Guo, D.; Lv, X. A THz detector chip with printed circular cavity as package and enhancement of antenna gain. *IEEE Trans. Antennas Propag.* **2016**, *64*, 1242–1249. [[CrossRef](#)]
29. Lepeshov, S.; Gorodetsky, A.; Krasnok, A.; Rafailov, E.; Belov, P. Enhancement of terahertz photoconductive antenna operation by optical nanoantennas. *Laser Photonics Rev.* **2017**, *11*, 1600199. [[CrossRef](#)]
30. Gric, T.; Gorodetsky, A.; Trofimov, A.; Rafailov, E. Tunable plasmonic properties and absorption enhancement in terahertz photoconductive antenna based on optimized plasmonic nanostructures. *J. Infrared Millim. Terahertz Waves* **2018**, *39*, 1028–1038. [[CrossRef](#)]
31. Guo, W.; Wang, L.; Chen, X.; Liu, C.; Tang, W.; Guo, C.; Wang, J.; Lu, W. Graphene-based broadband terahertz detector integrated with a square-spiral antenna. *Opt. Lett.* **2018**, *43*, 1647–1650. [[CrossRef](#)]
32. Ikamas, K.; Čibiraitė, D.; Lisauskas, A.; Bauer, M.; Krozer, V.; Roskos, H.G. Broadband terahertz power detectors based on 90-nm silicon CMOS transistors with flat responsivity up to 2.2 THz. *IEEE Electron Device Lett.* **2018**, *39*, 1413–1416. [[CrossRef](#)]
33. Gou, J.; Niu, Q.; Liang, K.; Wang, J.; Jiang, Y. Frequency modulation and absorption improvement of THz micro-bolometer with micro-bridge structure by spiral-type antennas. *Nanoscale Res. Lett.* **2018**, *13*, 1–9. [[CrossRef](#)] [[PubMed](#)]
34. Knap, W.; Deng, Y.; Romyantsev, S.; Lü, J.Q.; Shur, M.; Saylor, C.; Brunel, L. Resonant detection of subterahertz radiation by plasma waves in a submicron field-effect transistor. *Appl. Phys. Lett.* **2002**, *80*, 3433–3435. [[CrossRef](#)]
35. Knap, W.; Kachorovskii, V.; Deng, Y.; Romyantsev, S.; Lü, J.Q.; Gaska, R.; Shur, M.; Simin, G.; Hu, X.; Khan, M.A.; et al. Nonresonant detection of terahertz radiation in field effect transistors. *J. Appl. Phys.* **2002**, *91*, 9346–9353. [[CrossRef](#)]
36. Sakhno, M.; Golenkov, A.; Sizov, F. Uncooled detector challenges: Millimeter-wave and terahertz long channel field effect transistor and Schottky barrier diode detectors. *J. Appl. Phys.* **2013**, *114*, 164503. [[CrossRef](#)]

37. Gou, J.; Zhang, T.; Wang, J.; Jiang, Y. Spiral antenna-coupled microbridge structures for THz application. *Nanoscale Res. Lett.* **2017**, *12*, 91. [[CrossRef](#)]
38. Volakis, J.; Nurnberger, M.; Filipovic, D. Slot spiral antenna. *IEEE Antennas Propag. Mag.* **2001**, *43*, 15–26. [[CrossRef](#)]
39. Kramer, B.A.; Lee, M.; Chen, C.C.; Volakis, J.L. Design and performance of an ultrawide-band ceramic-loaded slot spiral. *IEEE Trans. Antennas Propag.* **2005**, *53*, 2193–2199. [[CrossRef](#)]
40. Dyson, J. The equiangular spiral antenna. *IRE Trans. Antennas Propag.* **1959**, *7*, 181–187. [[CrossRef](#)]
41. Yun-Fei, S.; Jan-Dong, S.; Xiao-Yu, Z.; Hua, Q.; Bao-Shun, Z.; Dong-Min, W. Enhancement of terahertz coupling efficiency by improved antenna design in GaN/AlGaIn high electron mobility transistor detectors. *Chin. Phys. B* **2012**, *21*, 108504.
42. Sakhno, M.; Gumenjuk-Sichevska, J.; Sizov, F. Modeling of THz detector antenna on conductive substrate. In Proceedings of the 2016 9th International Kharkiv Symposium on Physics and Engineering of Microwaves, Millimeter and Submillimeter Waves (MSMW), Kharkiv, Ukraine, 20–24 June 2016; pp. 1–3.